CHAPTER

12 Learning pathological deviations from a normal pattern of myocardial motion: Added value for CRT studies?

N. Duchateau[1], G. Piella[2], A. Frangi[3], M. De Craene[4]

Inria Sophia Antipolis, Sophia Antipolis, France[1] Universitat Pompeu Fabra, Barcelona, Spain[2]
University of Sheffield, Sheffield, United Kingdom[3] Philips Medisys, Suresnes,France[4]

CHAPTER OUTLINE

Machine Learning and Medical Imaging. http://dx.doi.org/10.1016/B978-0-12-804076-8.00012-8

12.1 INTRODUCTION

12.1.1 CARDIAC RESYNCHRONIZATION THERAPY

In the last decade, cardiac resynchronization therapy (CRT) has become the recommended procedure to treat heart failure in patients with asynchronous contraction of the cardiac chambers (Yu et al., 2006). A biventricular pacing device optimizes the left/right ventricular delay, and eventually the atrioventricular delay. When deficiencies in the conduction system are compensated, synchronous contraction is expected to improve the heart efficiency and patient survival. Established international guidelines recommend pacing patients with symptomatic heart failure, electrical abnormalities, and decreased left ventricular function (Brignole et al., 2013). Nonetheless, these selection criteria are suboptimal. The therapy fails to "improve enough" patient condition in approximately 30% of the cases (clinical response), and reverse remodeling in 50% of the cases (volume response) (Bleeker et al., 2006) This issue is of primary concern given the prevalence of the symptoms (between 25% and 50% of heart failure patients, at least 15 million people in Europe (van Veldhuisen et al., 2009)), and the associated costs (better implantation of 1% of the devices in the United States between 2003 and 2007 (Laskey et al., 2012) already means an impact of 105M€ to 15K€ per device, for 7000 devices).

Currently, no consensus exists on better selection criteria. Publications abound on new predictive indexes. Paradoxically, they focus too much on the blind assessment of mechanical dyssychrony (mainly through peak or time-to-event measurements), instead of better understanding the mechanisms of therapy response. A change towards a more comprehensive strategy was claimed more recently (Fornwalt, 2011) Some studies highlighted the relevance of distinguishing between specific types of dyssynchrony, each one associated with a pattern correctable by CRT (Parsai et al., 2009; Doltra et al., 2014) They pave the way towards interpreting those mechanical patterns in the light of precise electrical and structural abnormalities (Vernooy et al., 2014).

According to these findings, improving patient selection should therefore increase the recognition of these different types of dyssynchrony in new candidates.

12.1.2 PATTERNS OF MOTION/DEFORMATION

Myocardial motion and deformation can be extracted from cardiac sequences by combining segmentation and temporal registration/tracking. Local speckles attached to the myocardium allow tracking along 2D or 3D echocardiographic sequences and computing these parameters locally (Duchateau et al., 2013a) However, once temporal and anatomical variability are removed, the comparison of spatiotemporal patterns of motion and deformation is challenging.

Quantifying the distance from a patient to a normal motion pattern is an intuitive way of encoding pathological patterns. Clinicians actually do so when diagnosing a new patient: given the representation of a normal contraction (previously learnt), where and how much does the observed patient differ from normality? Then, once

categorized as abnormal, can a similar process be extended to quantify the distance to a known (ab)normal pattern?

This philosophy guided our work on dyssynchrony patterns amenable to CRT response. In a first instance, an atlas of normal motion was built from healthy subjects (Duchateau et al., 2011). The mean and covariance of myocardial velocities were encoded at each point of the myocardium. The motion of CRT candidates was locally compared to the atlas by a statistical distance to normality (p-value associated with the Mahalanobis distance). Motion abnormalities were coherent across subgroups of dyssynchrony patterns (Duchateau et al., 2012b) Notably, a specific pattern of intraventricular dyssynchrony (also called *septal flash*) predominated among the responders to the therapy, and mostly disappeared at mid-term follow-up. Qualitative observations previously reported that this pattern is associated with high response rates, if corrected (Parsai et al., 2009; Doltra et al., 2014).

In a second instance, we therefore intended to represent this specific pattern as a progressive deviation from normality (Duchateau et al., 2012a). We hypothesized that pattern variations were encoded in a nonlinear space of lower dimensionality, which could be modeled as a manifold. Then we proposed to quantify the distance between a new patient and this specific pattern, as a complement to its distance to normality. We expected that such distances could (before CRT) reflect the probability of response, and (after CRT) link the reduction in abnormality with the actual response (Duchateau et al., 2013c)

12.1.3 SUMMARY OF THE CHALLENGES

Due to the choice of a machine learning methodology for such a clinical application, we believe that three challenges should be highlighted:

- First, determining the *amount of preprocessing required* to study motion and deformation patterns. Features quality strongly impacts the performance of machine learning algorithms, although exaggerated efforts are often dedicated to their extraction. The literature abounds with methods to estimate myocardial motion via cardiac segmentation and tracking. Specific concrete physiological knowledge could refine the feature extraction in our application: local anatomical coordinates (radial, circumferential, and longitudinal), spatiotemporal a priori (phases of the cycle and anatomy should match), quasi-incompressibility of the cardiac motion (De Craene et al., 2012), etc. In addition to these specificities, we decided to precompute distances to a reference for normality to imitate the process of learning of clinicians, and enhance specific features of the motion patterns (Duchateau et al., 2012a).
- Then, knowing how to *"learn" a representation of a given pathology*. We believe that different grades of the same disease, for a patient or within a population, can be modeled as progressive impairments of a normal condition. We hypothesized that motion patterns belong or lie close to a nonlinear manifold that can be learnt from data by means of nonlinear dimensionality reduction.

Specific issues consist of choosing relevant learning techniques, depending on which feature characteristics to highlight, and comparing new subjects to this learnt representation.

- Finally, evaluating whether this representation is *useful* for the clinical application As indicated in Parsai et al. (2009) and Doltra et al. (2014), relating pattern changes to patient response is valuable for therapy planning. However, their assessment is currently qualitative or based on simple quantitative indexes. We therefore focused on demonstrating the value of our method to go beyond these limitations and quantify pattern-specific changes, to investigate if the pattern was fully or partially corrected after treatment.

12.2 FEATURES EXTRACTION: STATISTICAL DISTANCE FROM NORMAL MOTION

12.2.1 CONSTRUCTION OF ABNORMALITY MAPS

We chose to use myocardial velocity as a local descriptor for cardiac motion. This corresponds to small transformations that do not require elaborate computational anatomy techniques (Duchateau et al., 2011). Furthermore, the signature of the septal flash pattern shows greater contrast for velocities than displacements or strain patterns (Duchateau et al., 2014) These velocities are extracted from echocardiographic sequences by spatiotemporal registration (De Craene et al., 2012) or commercial speckle-tracking. These velocities are normalized both spatially and temporally to take into account differences in anatomy and in the timing of physiological events (Duchateau et al., 2011).

We decided to postprocess these data by highlighting values significantly different from normality (Fig. 12.1). This consists of three steps. At each location of the myocardium, the mean and covariance of velocities over a set of healthy volunteers encode a representation of local normal motion (the atlas in Duchateau et al. (2011)). Then, at the same locations, the velocity of each individual is compared to the distribution of velocity vectors for this reference population, using the Mahalanobis distance. Finally, the p-value associated with this distribution (assumed as Gaussian) encodes abnormality at each location: a low p-value indicates high abnormality and a p-value close to 1 stands for normal motion.

In our application, contrast in the abnormality maps is enhanced by using the logarithm of this p-value On top of this, the maps are multiplied by the sign of the radial velocity so that the characteristic pattern of septal flash is highlighted (the inward and outward motions of the septum during early diastole, Fig. 12.1).

12.2.2 WHICH STATISTICS FOR MOTION PATTERNS?

Voxel-based statistics are often used to analyze group-wise and inter-group differences after alignment to a common reference. Each voxel is considered independently

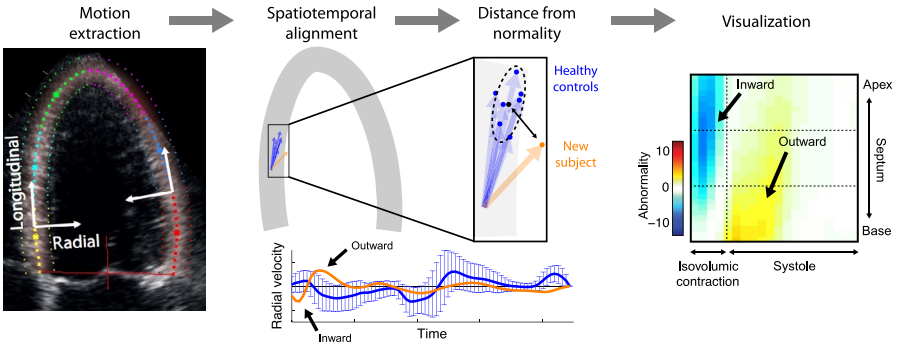

FIG. 12.1

Overview of the extraction of motion features, leading to the computation of spatiotemporal abnormality maps.

from the others, which may affect the statistical power of the results and bias conclusions. In our application, the link between neighboring regions cannot be discarded due to the nature of the data: mechanical tissue properties, regional noise patterns such as speckles, smoothness and temporal consistency of the extracted motion, etc.

Global statistics are also often retained. Methods search for an optimal space to compare subjects, according to specific criteria (eg, explaining the data variance, or discriminating groups of subjects). However, they often neglect the constraints of imaging data, in the sense that generalizations of the model should remain physiologically coherent.

When the structure of the data space is known (eg, the manifold of diffusion tensors or diffeomorphic transformations), mathematical operators exist to define statistics compliant with this space. In contrast, in our application, the structure of such a manifold should be learnt from data. We chose a specific nonlinear dimensionality reduction algorithm that is suitable when the data distribution is not clustered (Isomap; Tenenbaum et al., 2000). However, our framework is flexible and can easily be adapted to other embedding algorithms, which share similar principles (Yan et al., 2007).

12.3 MANIFOLD LEARNING: CHARACTERIZING PATHOLOGICAL DEVIATIONS FROM NORMALITY

Our dataset consists of 109 maps of abnormality like the one in Fig. 12.1, where rows and columns respectively correspond to the position along the septum and the time along the cycle. They were extracted from 2D echocardiographic sequences in a four-chamber view. Focus was kept on the isovolumic contraction (where septal

flash appears) and the systole. One map, completely synthetic, was filled with 0 values and served to encode true normality. The *learning set* was composed of this synthetic map and 50 real maps corresponding to a septal flash (Section 12.1). The *testing set* was made up of the remaining 58 real maps, corresponding to six cases with septal flash, 31 CRT candidates without septal flash, and 21 healthy volunteers.

The abnormality maps were considered as high-dimensional objects (20 dimensions for time × 31 dimensions for space), handled as column vectors by our method.

12.3.1 LEARNING PART: PATHOLOGICAL DEVIATIONS FROM NORMALITY (MANIFOLD LEARNING)

12.3.1.1 From high-dimensional motion patterns to low-dimensional coordinates (training set)

The Isomap algorithm (Tenenbaum et al., 2000) is used to reduce the dimensionality of the data while preserving a specific data arrangement. It maps each (high-dimensional) input sample to a space of (low-dimensional) coordinates where the Euclidean distance approximates the geodesic distance between two samples. One hypothesis is required: there is a low-dimensional manifold that can explain the main variations in the data.

The algorithm consists of three steps. First, input samples are connected via a nearest-neighbors search, using the Euclidean distance as metric. Then, the shortest path between each pair of samples is taken as surrogate for the geodesic distance, and stored in a matrix. Finally, this matrix is centered and diagonalized. Due to the matrix diagonalization and our initial hypotheses, dimensions of lower significance can be removed. This leads to a space of low-dimensional coordinates into which the geodesic distance is approximated by the Euclidean distance (Fig. 12.2). The top

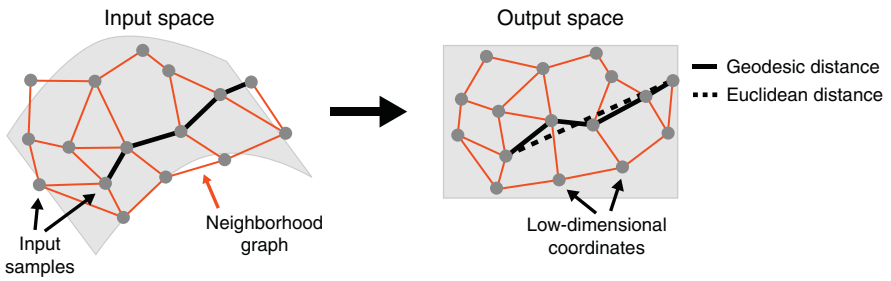

FIG. 12.2

Nonlinear dimensionality reduction via the Isomap algorithm.

Source: Adapted from Duchateau, N., De Craene, M., Piella, G., Frangi, A.F., 2012a. Constrained manifold learning for the characterization of pathological deviations from normality. Med. Image Anal. 16 (8), 1532–1549.

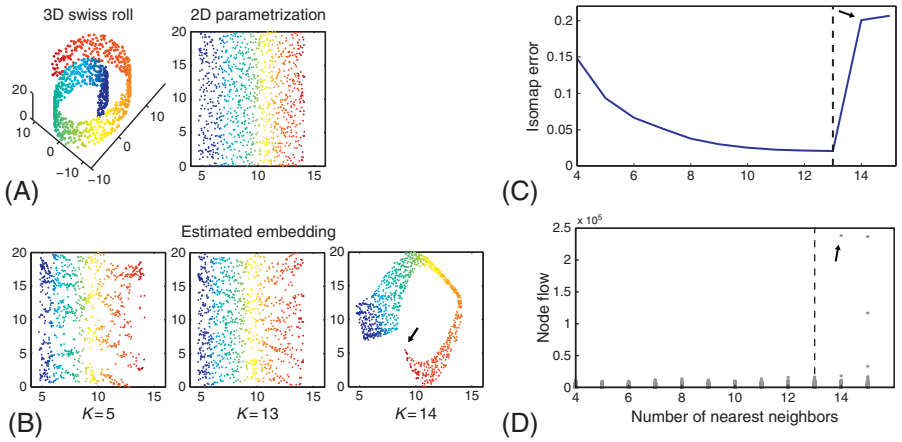

FIG. 12.3

(A) 3D Swiss roll and its associated 2D parameterization. (B)–(D) Influence of the number of nearest neighbors K (B) against the Isomap error (C) and the node flow (D), highlighting the apparition of a short-circuit (*black arrows*).

Source: Adapted from Duchateau, N., De Craene, M., Piella, G., Frangi, A.F., 2012a. Constrained manifold learning for the characterization of pathological deviations from normality. Med. Image Anal. 16 (8), 1532–1549.

N eigenvectors from the matrix diagonalization define the coordinates in this new N-dimensional space.

12.3.1.2 Tuning parameters

The algorithm starts building a graph of the training samples, by connecting nearest neighbors according to a given metric (in our case, the Euclidean distance). In this procedure, the number of neighbors needs to be determined. Synthetic experiments on the Swiss roll (Fig. 12.3) can show that the accuracy of the manifold estimation increases with the number of neighbors until a short-circuit occurs, which breaks the data arrangement. The ratio between the geodesic and the Euclidean distances (the *Isomap error*), computed in the output space, highlights the apparition of such a short-circuit (Fig. 12.3B). However, this measure may not be optimal on real data, in particular when the number of training samples is low.

We complemented this measure by the *node flow on a graph* (Choi and Choi, 2007), which reflects the number of shortest paths passing through each node of the graph. This measurement is directly performed on the graph, before any dimensionality reduction, and is therefore independent of the choice of dimensionality. A uniform arrangement of the training samples is reflected by the uniformity of the node flow distribution. In contrast, much higher node flow is observed at the nodes where a short-circuit occurs, as most of the shortest paths pass by this point (Fig. 12.3C).

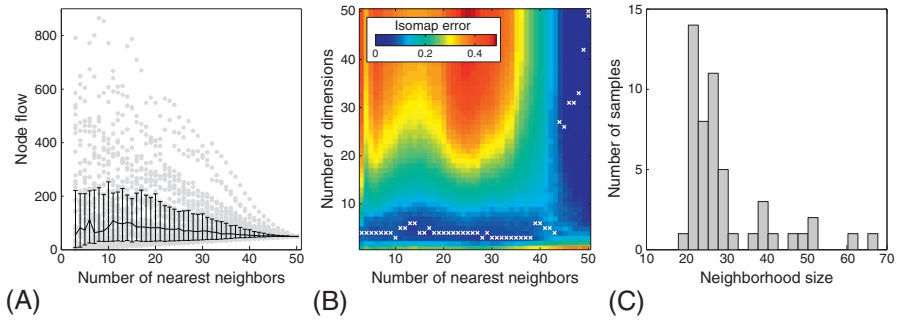

FIG. 12.4

(A) Node flow distribution against the number of nearest neighbors. Error bars indicate the median and first/third quartiles over the training set. (B) Isomap error against the dimensionality of the output space and the number of nearest neighbors. White crosses indicate the minimum value of each column. (C) Training set distribution of the neighborhood sizes (average distance between the five nearest neighbors).

Source: Adapted from Duchateau, N., De Craene, M., Piella, G., Frangi, A.F., 2012a. Constrained manifold learning for the characterization of pathological deviations from normality. Med. Image Anal. 16 (8), 1532–1549.

However, in this synthetic example, the dimensionality of the output space is known—the Swiss roll is a 2D plane embedded in a 3D space This is not the case for real data, and the number of dimensions of the output space should be estimated together with the number of nearest neighbors. Thus parameter estimation should start by checking the presence of a short-circuit by measuring the node flow, and then jointly evaluating the Isomap error against the dimensionality of the output space and the number of nearest neighbors. For our data, an increase in the number of neighbors did not point out the apparition of a short-circuit (Fig. 12.4A). According to the Isomap error (Fig. 12.4B), the dimensionality was set to 4. Few error changes were observed when using less than 30 neighbors, and this number was set to 5 to minimize the computational time.

The Isomap algorithm may be greatly affected by a heterogeneous density in the sample distribution, and in particular in the presence of "holes" in the distribution. This is partially the case for our data, as seen in Fig. 12.4C. For this aspect of learning, our method could be improved by algorithms that specifically target this robustness, such as diffusion maps (Coifman and Lafon, 2006). Note that similar concerns arise for the mapping part of our method, addressed in the following section.

12.3.1.3 Visualization: data spread and main directions

The first necessary checking consists of visualizing the low-dimensional embedding of the data. Two-dimensional representations such that in Fig. 12.5A are easily readable. The depicted patterns correspond to the abnormality maps of the training set.

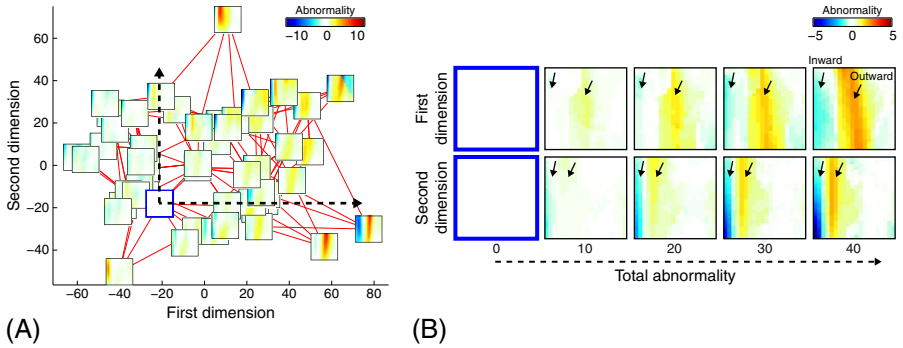

FIG. 12.5

(A) 2D visualization of the estimated embedding. The bold-framed map corresponds to the perfectly normal pattern used to constrain the manifold. (B) Progressive deviations from normality along the first two principal directions. The abnormal inward/outward motion pattern is preserved.

Source: Adapted from Duchateau, N., De Craene, M., Piella, G., Frangi, A.F., 2012a. Constrained manifold learning for the characterization of pathological deviations from normality. Med. Image Anal. 16 (8), 1532–1549.

We can qualitatively check that patterns are arranged in a coherent way, with more abnormal patterns on the border zone of the graph.

This information is complemented by Fig. 12.5B, where synthetic patterns were generated from coordinates evolving from normality along the first two dimensions (the dashed lines in Fig. 12.5A). Notably, the characteristic inward/outward events of the septal flash are preserved, while this is not the case with linear dimensionality reduction (Duchateau et al., 2012a) Note that this figure requires being able to reconstruct motion patterns from the low-dimensional coordinates, using the techniques described in Section 12.3.2.

12.3.2 TESTING PART: DISTANCES TO THE MODELED PATHOLOGY AND TO NORMALITY

12.3.2.1 From high-dimensional motion patterns to low-dimensional coordinates (testing set)

The low-dimensional coordinates associated with the motion pattern of a new subject can be estimated by means of nonlinear regression (Fig. 12.6A). We formulated it as an inexact matching problem using kernels—also referred to as ridge regression. The optimization looks for a "smooth enough" interpolating function (regularization term) that gets "close enough" to the training samples (similarity term). The kernel formulation both constrains the search into a given space of smooth functions (fixed by the kernel bandwidth) and provides an analytical solution to the

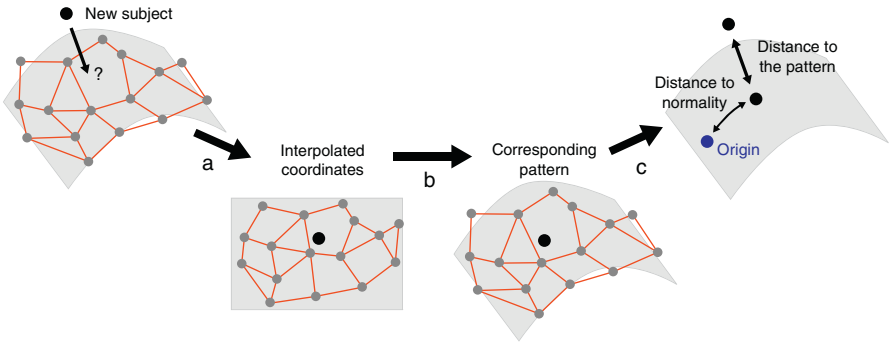

FIG. 12.6

Steps for comparing a new subject to the modeled pattern and to normality.

Source: Adapted from Duchateau, N., De Craene, M., Piella, G., Frangi, A.F., 2012a. Constrained manifold learning for the characterization of pathological deviations from normality. Med. Image Anal. 16 (8), 1532–1549.

interpolation problem. A scalar weight balances the contribution of the regularization and similarity terms.

To improve the quality of the mapping of new subjects, we adapted the methods in two ways.

First, our dataset includes a synthetic zero-valued abnormality map that encodes true normality (the bold map in Fig. 12.5). The interpolation problem is therefore adapted to an exact matching for this specific sample and an inexact matching for the remaining ones (Fig. 12.7A). This is simply addressed by modifying one matrix constraint in the analytical solution of the kernel regression.

Then, similarly to the learning algorithm of Section 12.3.1, this subpart of the algorithm is also sensitive to the nonuniform distribution of samples. Artifacts may arise from the use of a single-scale kernel, generally set to the average density of the samples Two methods were therefore tested:

- A *locally adjustable kernel* (Duchateau et al., 2012a), whose bandwidth is adapted to the local density of the samples, defined as the local neighborhood size. Although this approach provides robustness to local density variations, it deviates from the original formulation where a given kernel determines the space of functions where the problem is solved.
- A *multiscale strategy* (Duchateau et al., 2013b), where the interpolation process is iterated across scales, by dividing the kernel bandwidth by two at each iteration and interpolating the residual (Fig. 12.7B). This approach also has the advantage of removing one parameter from the method, as the kernel bandwidth is automatically determined, starting from the data spread to the average density of the samples.

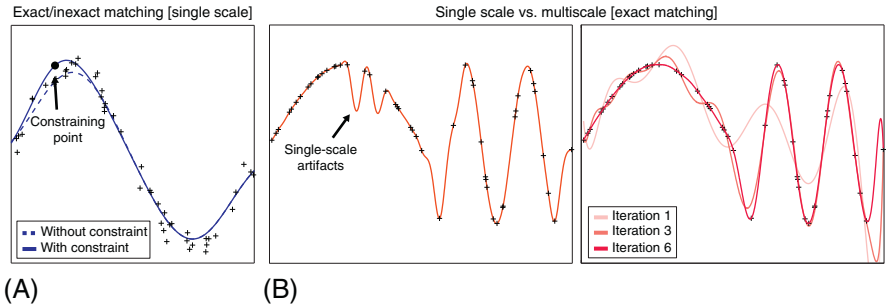

FIG. 12.7

(A) Single-scale interpolation without/with forcing the curve to pass by a given point.
(B) Robustness to local density variations: single- vs. multi-scale interpolation.
Source: Adapted from Duchateau, N., De Craene, M., Sitges, M., Caselles, V., 2013b. Adaptation of multiscale function extension to inexact matching. application to the mapping of individuals to a learnt manifold. In: SEE International Conference on Geometric Science of Information, LNCS. Springer, New York, with permission of Springer.

12.3.2.2 From low-dimensional motion coordinates to high-dimensional motion patterns (testing set)

The second part of the algorithm solves the reverse problem: it estimates the motion pattern that corresponds to the low-dimensional coordinates determined by the first step (Fig. 12.6B). The problem is formulated similarly, by switching the role of the motion patterns and the coordinates in the previous formulation.

12.3.2.3 Projection to the manifold and distances computation

As coordinates belong to the low-dimensional space associated with the manifold of motion patterns, all the patterns generated from these coordinates belong to the manifold. In the case of our application, the manifold is learnt from a population with a specific abnormal pattern, and all reconstructed data are expected to show this pattern (Fig. 12.5B). This means that any motion abnormality pattern can be "projected" to the manifold by the combination of these two interpolations. In other words, the method estimates the element of the manifold that shares coordinates with a tested individual, possibly out of this manifold.

Two distances are defined (Fig. 12.6C):

- A distance between any abnormality map and the manifold (*distance to the manifold*), which quantifies how far a given subject is from the modeled abnormal pattern. This corresponds to the total error between a given abnormality map and its reconstruction.
- A *distance to normality*. This corresponds to the Euclidean distance between the coordinates of the new subject and the origin—the synthetic map defining true normality.

Table 12.1 Determination of the Main Parameters for Our Method

Parameter	Estimation Method	Concerned Set
Number of nearest neighbors	Node flow + Isomap error	Training
Dimensionality of the output space	Node flow + Isomap error	Training
Kernel bandwidth	Distribution of neighborhood sizes + adaptive kernel or multiscale formulation	Testing
Interpolation weight	Generalization ability	Testing
Sample size	Convergence of the results	Training + testing

12.3.2.4 Tuning parameters

As for the learning part of the algorithm, the method parameters need to be estimated. Each interpolation depends on a kernel bandwidth and a regularization weight. Kernel bandwidths are automatically determined (Section 12.3.2). The regularization weights for the two consecutive interpolations are jointly estimated by heuristic tests. Their optimal values are determined based on the generalization ability over the training set—the reconstruction error when using a leave-one-out approach (Davies et al., 2010) In our application, they corresponded to 10^1 and $10^{0.5}$ respectively (Duchateau et al., 2012a).

Naturally, the performance of the methods depends on the size of the training population. The two estimated distances (to the manifold and to normality) were computed from randomly generated datasets of smaller size. Convergence was assessed by the number of subjects above which the results stabilize to their final value $\pm 5\%$: above 45 subjects for the distance to the manifold and above 41 subjects for the distance to normality (Duchateau et al., 2012a). Both indicate that results on our population of 50 real subjects can be trusted.

A summary of the estimation of the method parameters is given in Table 12.1.

12.4 BACK TO THE CLINICAL APPLICATION: UNDERSTANDING CRT-INDUCED CHANGES

The motion patterns of our population were analyzed with respect to the two proposed distances: the distance to the manifold, which models the abnormal pattern of septal flash, and the distance to normality along the manifold. These distances define a 2D space where subgroup differences can easily be visualized (Fig. 12.8), as discussed below.

12.4.1 ANALYSIS PER POPULATION

We first checked that the two distances provided a meaningful organization of all the data at baseline.

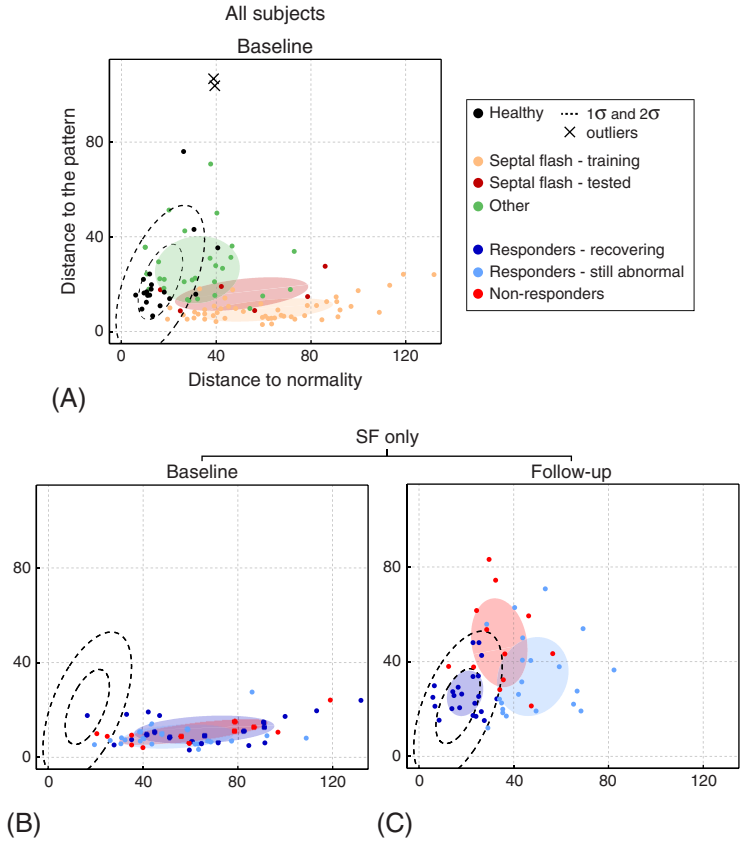

FIG. 12.8

Subjects distribution according to the distances to the modeled pattern and to normality. Dashed lines indicate the normality range defined by the healthy population.

Source: Adapted from Duchateau, N., Piella, G., Doltra, A., Mont, L., Bijnens, B.H., Sitges, M., De Craene, M., 2013c, Manifold learning characterization of abnormal myocardial motion patterns: application to crt-induced changes. In: Ourselin, S., Rueckert, D., Smith, N. (Eds.), Proceedings of Functional Imaging and Modeling of the Heart, LNCS, vol. 7945. Springer, New York, pp. 450–457. With permission of Springer.

The training set, made of septal flash cases, has a low distance to the modeled pattern. This actually reflects the reconstruction error of the interpolations, formulated as an inexact matching. Such cases spread all along the horizontal axis from low to high abnormal patterns, which also indicates that the whole support of the manifold defines the distance to normality. Few of them are close to the origin for normality, which may arise from the accuracy of the septal flash diagnosis and the accuracy of the abnormality maps to detect low-grade abnormalities.

Among the testing set, patients with septal flash are mapped close to the training cases, according to their respective abnormality. Volunteers lie close from the origin

for normality. Two subjects are outliers (black crosses out of the dashed ellipse). They correspond to cases with high abnormalities due to high velocities despite a normal pattern, lying out of the range of the other healthy subjects. Their pattern of abnormality cannot be reconstructed by the training set of septal flash cases, which leads to a large distance to the modeled pattern. Similarly, patients with an abnormal pattern different from septal flash are mapped far from the manifold, and out of the normality range.

12.4.2 LINK WITH CRT RESPONSE

The manifold is exclusively learnt from septal flash patterns. When looking at individual evolutions with CRT, our method only evaluates if a studied pattern (not necessarily septal flash) got closer to septal flash or normality. If the pattern is different from septal flash, we cannot tell if this pattern is still present or not. Thus we focused the outcome analysis on the subjects diagnosed with septal flash at baseline (Fig. 12.8B and C).

Patients were separated according to the volume response to CRT, measured by a clinical expert as a reduction $\geq$15% in left-ventricular end-systolic volume, without heart transplantation Three subgroups were identified: responders who recovered normal motion at follow-up (who were within the normality range defined by the healthy subjects), responders for which abnormal motion is still present, and nonresponders.

These subgroups cannot be distinguished at baseline: the presence of septal flash at baseline is not a sufficient condition for CRT response. This coincides with the philosophy of Parsai et al. (2009) and Doltra et al. (2014), which interpreted response at follow-up in light of the correction of the identified abnormal mechanisms. In our population, significant changes are visible at follow-up. Patients within the range of normal motion are mostly responders. The other patients have higher distance to the manifold, suggesting that septal flash may have disappeared. However, their abnormalities are still high, which may explain their lack of response. Beyond these qualitative interpretations, the number of changes can be quantified with our method and can further be related with quantitative indexes of therapy outcome.

Further results and discussion can be found in Duchateau et al. (2013c). They notably include the evolution of the whole population, and the outcome immediately after pacing Complementary interpretations are also given in Duchateau et al. (2012a), which points out the limitations of a linear analysis (principal compound analysis, PCA) and the meaning of the proposed distances against the total abnormality in each map.

12.5 DISCUSSION/FUTURE WORK

We presented a method to model pathological myocardial motion patterns as a smooth deviation from normality, along a nonlinear manifold structure, learnt from data. This representation gives a comparison of new samples to the modeled pattern

and to normality, and provides quantitative insights into the mechanisms of CRT response.

12.5.1 PATTERN-BASED COMPARISONS

Regarding technical aspects, our main contribution resides in the methodology to compare myocardial motion patterns. Previous work used atlas tools to align data in time and space, and to enhance the contrast in the features of interest by a statistical comparison to normality at each voxel (Duchateau et al., 2011). These tools already facilitated the quantitative analysis of CRT response, by highlighting the prevalence and the correction of specific abnormal patterns in groups of responders and nonresponders. In this chapter, we illustrated the potential of the pattern-wise comparisons proposed in Duchateau et al. (2012a). Pattern variations now model the spatiotemporal interdependences in the data. Furthermore, the proposed distances provide physiologically coherent support to the interpretation of the patterns' evolution with therapy.

The methodology is based on standard manifold learning and nonlinear regression. Improvements could be made on several parts of the pipeline, depending on the application targeted: getting more power out of the metrics, adding robustness to the density of the samples during learning, combining features of different types (Sanchez-Martinez et al., 2015), modeling several abnormal patterns at once, etc. The pipeline is easily transposable to other applications, imaging modalities, and features of interest (not necessarily in cardiac imaging). However, the main decision should be taken as early as possible, to decide whether using a similar but complex framework (statistical atlas and learning a manifold) can add value to the clinical application. In our case, there was a clear claim for the quantitative analysis of dyssynchrony patterns amenable to CRT response (Fornwalt, 2011), and a convergence of clinical studies towards mechanistic approaches (Parsai et al., 2009), which was subsequently confirmed (Doltra et al., 2014). 2D echocardiographic data were retained due to the wide implantation of the modality in clinical routine and CRT monitoring. The high temporal resolution and the easy checking of 2D echocardiographic data outputs also facilitated this decision, when 3D data were not straightforward to handle.

12.5.2 GOING BEYOND PARSAI'S PAPER?

The results in Parsai et al. (2009) had already led to a great improvement in CRT, as the decision algorithm improved patient selection by removing ambiguity on three out of five groups, which always or never respond. Simple criteria defined the inclusion to a given group and facilitated the reproducibility of the results. Our methodology is more difficult to implement in clinical routines, and simpler but comprehensive indexes that characterize dyssynchrony patterns may be more relevant in this context. However, our approach allows quantification of pattern evolution with therapy, which would not be straightforward with the indexes in (Parsai et al., 2009), in particular if the pattern is highly modified.

The results in Parsai et al. (2009) also offered a broader view on the way to treat dyssynchrony. Intraventricular dyssynchrony is purely electrical, meaning that resynchronization should lead to a response in subjects with septal flash, therefore defining a hyperresponders population. In contrast, structural disease on top of the electrical abnormalities worsens the outcome: although electrical dyssynchrony is corrected, mechanical abnormalities (myocardial infarct) still exist and the probability of response is highly decreased Going beyond these interpretations, confirmed by our results, should consider additional variety in these mechanisms. External factors could affect the clinical condition, such as the presence of atrial fibrillation, the lack of contractile reserve, or the lead position, and should be considered in future studies. Nonetheless, from a learning perspective, the user should always keep in mind the amount of effort required to extract features of interest for these data.

Finally, one of the strongest limitations to CRT resides in the definition of response. Paradoxically, no agreement exists (Fornwalt et al., 2010) We hope that our approach, based on the quantification of abnormality, can open the way towards less binary views of the success of the therapy. Further studies should evaluate the added value of a continuous spectrum of responses, which may include measures of abnormality evolution with the therapy.

ACKNOWLEDGMENTS

This work was done between 2008 and 2013 with the partial support of the Spanish Industrial and Technological Development Center (CDTeam and cvREMOD CEN-20091044), the Spanish Ministry of Science and Innovation, Plan E and ERDF (STIMATH TIN2009-14536-C02-01), and the European Commission's 7th Framework Program (euHeart FP7-ICT-224495). The authors acknowledge the contribution of their co-authors on related publications, in particular those from Bart Bijnens (ICREA, Universitat Pompeu Fabra, Barcelona, Spain) and Marta Sitges (Hospital Clínic, Barcelona, Spain) on clinical applications, and Vicent Caselles (Universitat Pompeu Fabra, Barcelona, Spain) on aspects of density invariance.

REFERENCES

Bleeker, G.B., Bax, J.J., Fung, J.W., van der Wall, E.E., Zhang, Q., Schalij, M.J., Chan, J.Y., Yu, C.M., 2006. Clinical versus echocardiographic parameters to assess response to cardiac resynchronization therapy. Am. J. Cardiol. 97 (2), 260–263.

Brignole, M., Auricchio, A., Baron-Esquivias, G., Bordachar, P., Boriani, G., Breithardt, O.A., Cleland, J., Deharo, J.C., Delgado, V., Elliott, P.M., Gorenek, B., Israel, C.W., Leclercq, C., Linde, C., Mont, L., Padeletti, L., Sutton, R., Vardas, P.E., ESC Committee for Practice Guidelines (CPG), Zamorano J.L., Achenbach, S., Baumgartner, H., Bax, J.J., Bueno, H., Dean, V., Deaton, C., Erol, C., Fagard, R., Ferrari, R., Hasdai, D., Hoes, A.W., Kirchhof, P., Knuuti, J., Kolh, P., Lancellotti, P., Linhart, A., Nihoyannopoulos, P., Piepoli, M.F., Ponikowski, P., Sirnes, P.A., Tamargo, J.L., Tendera, M., Torbicki, A.,

Wijns, W., Windecker, S., Document Reviewers: Kirchhof, P., Blomstrom-Lundqvist, C., Badano, L.P., Aliyev, F., Bansch, D., Baumgartner, H., Bsata, W., Buser, P., Charron, P., Daubert, J.C., Dobreanu, D., Faerestrand, S., Hasdai, D., Hoes, A.W., Le Heuzey, J.Y., Mavrakis, H., McDonagh, T., Merino, J.L., Nawar, M.M., Nielsen, J.C., Pieske, B., Poposka, L., Ruschitzka, F., Tendera, M., Van Gelder, I.C., Wilson, C.M., 2013. 2013 ESC guidelines on cardiac pacing and cardiac resynchronization therapy. Eur. Heart J. 34 (29), 2281–2329.

Choi, H., Choi, S., 2007. Robust kernel isomap. Pattern Recogn. 40 (3), 853–862.

Coifman, R., Lafon, S., 2006. Diffusion maps. Appl. Comput. Harmon. Anal. 21 (1), 5–30.

Davies, R.H., Twining, C.J., Cootes, T.F., Taylor, C.J., 2010. Building 3-d statistical shape models by direct optimization. IEEE Trans. Med. Imaging 29 (4), 961–981.

De Craene, M., Piella, G., Camara, O., Duchateau, N., Silva, E., Doltra, A., D'hooge, J., Brugada, J., Sitges, M., Frangi, A.F., 2012. Temporal diffeomorphic free-form deformation: application to motion and strain estimation from 3d echocardiography. Med. Image Anal. 16 (2), 427–450.

Doltra, A., Bijnens, B., Tolosana, J.M., Borràs, R., Khatib, M., Penela, D., De Caralt, T.M., Castel, M.Á., Berruezo, A., Brugada, J., Mont, L., Sitges, M., 2014. Mechanical abnormalities detected with conventional echocardiography are associated with response and midterm survival in CRT. JACC Cardiovasc. Imaging 7 (10), 969–979.

Duchateau, N., De Craene, M., Piella, G., Silva, E., Doltra, A., Sitges, M., Bijnens, B.H., Frangi, A.F., 2011. A spatiotemporal statistical atlas of motion for the quantification of abnormalities in myocardial tissue velocities. Med. Image Anal. 15 (3), 316–328.

Duchateau, N., De Craene, M., Piella, G., Frangi, A.F., 2012a. Constrained manifold learning for the characterization of pathological deviations from normality. Med. Image Anal. 16 (8), 1532–1549.

Duchateau, N., Doltra, A., Silva, E., De Craene, M., Piella, G., Castel, M.Á., Mont, L., Brugada, J., Frangi, A.F., Sitges, M., 2012b. Atlas-based quantification of myocardial motion abnormalities: added-value for understanding the effect of cardiac resynchronization therapy. Ultrasound Med. Biol. 38 (12), 2186–2197.

Duchateau, N., Bijnens, B.H., D'hooge, J., Sitges, M., 2013a. Three-dimensional assessment of cardiac motion and deformation, second ed. CRC Press, Boca Raton, FL. pp. 201–213.

Duchateau, N., De Craene, M., Sitges, M., Caselles, V., 2013b, Adaptation of multiscale function extension to inexact matching. Application to the mapping of individuals to a learnt manifold, LNCS. In: SEE International Conference on Geometric Science of Information. Springer, New York.

Duchateau, N., Piella, G., Doltra, A., Mont, L., Bijnens, B.H., Sitges, M., De Craene, M., 2013c, Manifold learning characterization of abnormal myocardial motion patterns: application to CRT-induced changes. In: Ourselin, S., Rueckert, D., Smith, N. (Eds.), Proceedings of Functional Imaging and Modeling of the Heart, LNCS, vol. 7945. Springer, New York, pp. 450–457.

Duchateau, N., Sitges, M., Doltra, A., Fernández-Armenta, J., Solanes, N., Rigol, M., Gabrielli, L., Silva, E., Barceló, A., Berruezo, A., Mont, L., Brugada, J., Bijnens, B., 2014. Myocardial motion and deformation patterns in an experimental swine model of acute LBBB/CRT and chronic infarct. Int. J. Cardiovasc. Imaging 30 (5), 875–887.

Fornwalt, B.K., 2011. The dyssynchrony in predicting response to cardiac resynchronization therapy: a call for change. J. Am. Soc. Echocardiogr. 24 (2), 180–184.

Fornwalt, B.K., Sprague, W.W., BeDell, P., Suever, J.D., Gerritse, B., Merlino, J.D., Fyfe, D.A., León AR, O.J., 2010. Agreement is poor among current criteria used to define response to cardiac resynchronization therapy. Circulation 121 (18), 1985–1991.

Laskey, W., Awad, K., Lum, J., Skodacek, K., Zimmerman, B., Selzman, K., Zuckerman, B., 2012. An analysis of implantable cardiac device reliability. the case for improved postmarketing risk assessment and surveillance. Am. J. Therap. 19 (4), 248–254.

Parsai, C., Bijnens, B., Sutherland, G.R., Baltabaeva, A., Claus, P., Marciniak, M., Paul, V., Scheffer, M., Donal, E., Derumeaux, G., Anderson, L., 2009. Toward understanding response to cardiac resynchronization therapy: left ventricular dyssynchrony is only one of multiple mechanisms. Eur. Heart J. 30 (8), 940–949.

Sanchez-Martinez, S., Duchateau, N., Bijnens, B., Erdei, T.and Fraser, A., Piella, G., 2015. Characterization of myocardial motion by multiple kernel learning: application to heart failure with preserved ejection fraction. In: van Assen, H., Bovendeerd P., Delhaas, T. (Eds.), Proceedings of Functional Imaging and Modeling of the Heart, LNCS vol. 9126. springer, New York, pp. 65–73.

Tenenbaum, J.B., de Silva, V., Langford, J.C., 2000. A global geometric framework for nonlinear dimensionality reduction. Science 290 (5500), 2319–2323.

van Veldhuisen, D.J., Maass, A.H., Priori, S.G., Stolt, P., van Gelder, I.C., Dickstein, K., Swedberg, K., 2009. Implementation of device therapy (cardiac resynchronization therapy and implantable cardioverter defibrillator) for patients with heart failure in Europe: changes from 2004 to 2008. Eur. J. Heart Fail. 11 (12), 1143–1151.

Vernooy, K., van Deursen, C.J., Strik, M., Prinzen, F.W., 2014. Strategies to improve cardiac resynchronization therapy. Nat. Rev. Cardiol. 11 (8), 481–493.

Yan, S., Xu, D., Zhang, B., Zhang, H.J., Yang, Q., Lin, S., 2007. Graph embedding and extensions: a general framework for dimensionality reduction. IEEE Trans. Pattern Anal. Mach. Intell. 29 (1), 40–51.

Yu, C.M., Hayes, D.L., Auricchio, A., 2006. Cardiac Resynchronization Therapy. Wiley-Blackwell, New York.